2014

Enhanced depth-independent chondrocyte proliferation and phenotype maintenance in an ultrasound bioreactor and an assessment of ultrasound dampening in the scaffold

Sanjukta Guha Thakurta
University of Nebraska-Lincoln

Mikail Kraft
University of Nebraska-Lincoln

Hendrik J. Viljoen
University of Nebraska-Lincoln, hviljoen1@unl.edu

Anuradha Subramanian
University of Nebraska - Lincoln, asubramanian2@unl.edu

Published in *Acta Biomaterialia* 10:11 (2014), pp. 4798-4810; doi: 10.1016/j.actbio.2014.07.013
Published by Elsevier Ltd. on behalf of Acta Materialia Inc. Used by permission.
Submitted January 8, 2014; revised July 11, 2014; accepted July 14, 2014, published online July 25, 2014.

Enhanced depth-independent chondrocyte proliferation and phenotype maintenance in an ultrasound bioreactor and an assessment of ultrasound dampening in the scaffold

Sanjukta Guha Thakurta, Mikail Kraft, Hendrik J. Viljoen, and Anuradha Subramanian

Department of Chemical Engineering, 207L Othmer Hall, University of Nebraska-Lincoln, Lincoln, NE 68588-0643, USA

Corresponding author – Anuradha Subramanian, email asubramanian2@unl.edu

Abstract
Chondrocyte-seeded scaffolds were cultured in an ultrasound (US)-assisted bioreactor, which supplied the cells with acoustic energy around resonance frequencies (~5.0 MHz). Polyurethane-polycarbonate (BM), chitosan (CS) and chitosan–n-butanol (CSB) based scaffolds with varying porosities were chosen and the following US regimen was employed: 15 kPa and 60 kPa, 5 min per application and 6 applications per day for 21 days. Non-stimulated scaffolds served as control. For BM scaffolds, US stimulation significantly impacted cell proliferation and depth-independent cell population density compared to controls. The highest COL2A1/COL1A1 ratios and ACAN mRNA were noted on US-treated BM scaffolds compared to controls. A similar trend was noted on US-treated cell-seeded CS and CSB scaffolds, though COL2A1/COL1A1 ratios were significantly lower compared to BM scaffolds. Expression of Sox-9 was also elevated under US and paralleled the COL2A1/COL1A1 ratio. As an original contribution, a simplified mathematical model based on Biot theory was developed to understand the propagation of the incident US wave through the scaffolds and the model analysis was connected to cellular responses. Scaffold architecture influenced the distribution of US field, with the US field being the least attenuated in BM scaffolds, thus coupling more mechanical energy into cells, and leading to increased cellular activity.

Keywords: Tissue engineering, Chondrocyte, Bioreactor, Low-intensity continuous ultrasound, Ultrasound dampening

1. Introduction

The field of tissue engineering promises to yield substitutes that could potentially overcome the limited availability of native explants [1–3]. For example, tissue engineered neo-cartilage with appropriate biomechanical properties holds promise both for graft applications and as a model system for controlled studies of chondrogenesis [4, 5]. Research into the "engineering aspects" of cartilage-tissue equivalents typically involves the fabrication of scaffold, design and evaluation of appropriate bioreactors, and controlling stem-cell fate to produce an alternative source of cells [6, 7]. Currently, all aspects of the tissue engineering process are being intensively researched, starting with the choice of cell source, cell selection, in vitro cell expansion, scaffold design, cell seeding and bioreactor cultivation and conditioning [8–11]. Typically, many of these aspects are interrelated. For example, while bioreactors are mainly designed to alleviate mass-transfer limitations, they also provide mechanical conditioning to the developing tissue and impact cell colonization depending upon the scaffold microstructure [12–16]. The long-term research objective is to achieve uniform cell distribution and cell differentiation throughout the scaffold volume so that a robust tissue, both biochemically and biomechanically, may be generated.

To obtain uniform cell colonization and cellular ingrowth into the thickness of the scaffold over the duration of culture, scaffold designs offering highly interconnected and accessible pore networks are often fabricated. Most of the scaffolds used in current tissue engineering applications possess pore diameters ranging from 50 to 500 μm, with a total porosity of 48–95% [17]. Other features indicative of successful cell infiltration include pore interconnectivity/tortuosity and scaffold permeability. We note that reduced pore connectivity may indicate closed pores, thus limiting the route for colonization with duration of culture.

Factors that impact cell colonization other than the structural features of scaffold are: (i) the cell seeding method employed which controls the initial spatial distribution of cells; and (ii) mechanical conditioning of the cell–scaffold construct during culture [11, 18, 19]. In the static surface seeding method, where the cells are first evenly layered on top of the scaffold and cultured, variable results were obtained and many studies report non-uniform cellular distributions [20]. To better exploit the principle of convective transport of cells in scaffold seeding, perfusion of cell suspensions through porous polymeric foams

in flow bioreactor or under orbital shaking and centrifugation was investigated [18], [21–23]. Variable results have been attained with dynamic seeding; orbital shaking has been noted to yield the highest spatial distribution of cells in the construct at 7 days in culture [21]. In general, static or dynamic cell-seeding methods used in conjunction with perfusion bioreactors yield a uniform initial cell distribution.

Conditioning of cell-seeded constructs during culture offers several important advantages compared to static culture systems, such as enhanced mass transfer of O_2 and nutrients by convective fluid flow, the ability to provide mechanical forces influencing tissue development, and better control over culture conditions [24]. The flow of medium through the scaffold porosity benefits cell differentiation by enhancing nutrient transport to the scaffold interior and by providing mechanical stimulation to cells in the form of fluid shear [25, 26].

Our previous work has shown that the stimulation of in vitro chondrocyte cultures by low-intensity continuous ultrasound (US) can modulate the signal-transduction pathways leading to chondrocyte-specific gene regulation or RNA translation of a protein product, or both [27, 28]. Thus, to capitalize on the positive bioeffects of low-intensity continuous US and apply them to the field of cartilage tissue engineering, our laboratory has designed and developed an ultrasonic bioreactor configuration that uses US to stimulate chondrocytes maintained in an in vitro culture [29]. Aspects of US that would negatively affect cells, including temperature and cavitation, were shown to be insignificant for the US protocols used covering a wide range of frequencies and pressure amplitudes, including the ones used in the present study.

This paper has two research focuses. First, we assess whether culturing chondrocyte-seeded scaffold under low-intensity continuous US stimulation in an US-assisted bioreactor that supplies the cells with acoustic energy around resonance frequencies can yield uniform cell proliferation and cell population density throughout the porous scaffold. Second, we investigate whether the spatial architecture of scaffold and US stimulation can regulate post-expansion redifferentiation and maintenance of chondrocyte phenotype. We posit that the use of the US-assisted bioreactor will result in a higher cell population density throughout the scaffold volume by preventing peripheral encapsulation, and coupled with mechanical stimulation of the cells, will result in an improved chondrogenic response by the bovine articular chondrocytes (BAC) cells cultured on scaffolds.

For the current study, we have used (i) chitosan (CS) scaffolds fabricated via the conventional freeze–drying–lyophilization (FDL) process [30, 31]; (ii) chitosan-10% n-Butanol scaffolds with improved porosity prepared via the emulsion FDL [32]; and (iii) polycarbonate–polyurethane-based elastomeric scaffold, a generous gift from Biomerix Corporation, CA. We have employed a static surface-seeding method to minimize the orthogonal effects of flow-assisted cell seeding. We assessed cell proliferation with respect to US stimulation and culture duration. Next, we have evaluated cell population density (i.e. an indirect measure of cell proliferation) at a given depth in the axial direction of the scaffold and their distribution on a particular scaffold via image analysis obtained with confocal microscoscopy. We observed cell morphology with scanning electron microscopy (SEM). Our studies are supported with gene expression analyses for Collagen 1A1, Collagen 2A1, Sox-9, Aggrecan, Collagen 10A1, TGFβ1 and TGFβ3 via real-time quantitative reverse transcription polymerase chain reaction (qRT-PCR), and protein expression analyses for Collagen 1A1, Collagen 2A1, Sox-9 and Aggrecan protein expression by Western blotting. To better explain the experimentally observed cellular distributions, we developed a simplified mathematical model based on Biot theory that (i) captures the essential interactions to predict the propagation of the incident US wave through the scaffolds with different geometries, and (ii) assesses the dampening of the US in the scaffold and, finally, connects the analysis to cellular responses.

2. Materials and methods

2.1. Reagents

Unless otherwise specified, all reagents were of analytical grade or better and were purchased from Sigma Aldrich. CS with a degree of deacetylation of 83% was purchased from Vanson (Redmond, WA) and used without further purification. A polycarbonate polyurethane-based scaffold (Biomerix 3D Scaffold™) was a generous gift from Biomerix, Inc. (Freemont, CA) and is denoted as BM.

2.2. Scaffold preparation

CS scaffolds were prepared by the FDL method detailed elsewhere [30, 31]. In parallel, CS was also mixed with 10 vol.% n-butanol and the resultant scaffolds (denoted as CSB) were prepared by emulsion FDL [32]. The CS, CSB and BM scaffolds were cut with a biopsy punch into specimens of 5 mm × 2.5 mm (diameter × thickness). CS and CSB scaffolds were neutralized with 0.25 M NaOH followed by thorough rinsing with deionized water. BM, and neutralized CS and CSB scaffolds were either directed to the scaffold sterilization step or dried in the lyophilizer for material characterization.

2.3. Characterization of scaffolds

2.3.1. Variable-pressure scanning electron microscopy (VPSEM)

The morphologies of the scaffolds were characterized by VPSEM (Hitachi S-3000N) at the Center of Biotechnology, University of Nebraska-Lincoln (Lincoln, NE) following the standard procedure detailed elsewhere [33]. Pore diameters were measured using image analysis software (ImageJ™, National Institutes of Health, USA).

2.3.2. Mercury intrusion porosimetry (MIP)

MIP measurements were performed at the Materials Science and Engineering Research Facility at the University of Washington (Seattle, WA). A Micromeritics Autopore IV 9500 porosimeter was used to analyze the samples and Autopore IV software was used to generate pore-related data.

2.4. Cell culture

2.4.1. Bovine chondrocyte isolation and culture

Bovine articular chondrocytes (BACs) were isolated using the standard procedure detailed elsewhere [33]. Frozen cell stocks were thawed and expanded in RPMI 1640 medium supplemented with 10% FBS, 2 g $NaHCO_3$, 1 mM sodium pyruvate, 1 mM antibiotic–antimycotic and 25 μg ml^{-1} L-ascorbic acid. The same medium was used in the culture of cell-seeded constructs. Cultures were maintained at 37 °C under a 5% CO_2 humidified atmospheric chamber. Passage 2 cells were serum deprived for 24 h by replacing 10% FBS with 0.1% FBS in the culture medium, trypsinized and used in all cell-seeding experiments.

2.4.2. Scaffold sterilization and cell seeding

CS, CSB and BM scaffolds were sterilized with sequential treatments of 70% and 90% ethanol solution for 1 h followed by sterile 1× PBS rinse and incubation in cell culture medium

(RPMI with 10% FBS) for 12 h. Prewetted scaffold disks were seeded with bovine chondrocytes at a seeding density of 2×10^4 cells per scaffold by pipetting cell suspension onto a side of each scaffold (Figure 1) and placed in the incubator for 4 h to facilitate cell adhesion. Scaffolds were then transferred to a new 6-well TCP plate housing a cellcrown™ insert/well with 15–18 scaffolds per insert. 8 ml of fresh RPMI media was added per well and subjected to US stimulation. One plate with 90–108 scaffolds represented one test condition.

2.4.3. Ultrasound-assisted bioreactor

A US-assisted bioreactor configuration that is detailed elsewhere was employed to provide US stimulation [29]. As described in Figure 1, TCP plates with cell-seeded scaffolds were placed in the bioreactor (i.e. plate holders), and US was applied according to the indicated regimen (Table 1). Non-stimulated cell-seeded scaffolds served as control and were handled similarly to the US-treated specimens. The medium was changed every 2–3 days. At the end of 1, 7, 14 and 21 days, scaffolds from each study group were randomly harvested from the plates and subjected to evaluation as detailed.

2.5. Tissue engineering construct (TEC) characterization

2.5.1. Visualization of cell distribution

Cell-seeded scaffolds were fixed with 4% paraformaldehyde. To visualize the nucleus, construct were permeabilized with 0.1% Triton X-100 (in 1× TBS), followed by blocking with 1% bovine serum albumin (BSA) in 1× TBST, and incubating with 1:5000 dilution of Sytox. Finally, the cylindrical scaffolds were rinsed thoroughly with 1× TBST, cut diametrically in the middle along the *x*–*z* plane (Figure 2b) and imaged with an inverted confocal microscope (Olympus IX 81) at 4× magnification (Z step size = 5 μm). Optical sections were merged and used for further image analysis. The green color represented nuclei. Three randomly selected scaffolds were imaged per study group.

2.5.2. In vitro cell distribution estimation

Confocal images were analyzed with ImageJ™ according to the method shown in Figure 2. Selected areas at the top, middle and bottom sections of a scaffold (Figure 2d) were analyzed to yield the cell population density (cells per unit area, ρ) which is the ratio of the total area occupied by the cells (green dots) to the total area of selected section. Automatic thresholding was applied to the sections analyzed. The total area covered by the green dots in each individual section, which represents the nuclei, was computed using the analyze particle command assuming size: 0–∞ and circularity 0.5–1.0 [34]. The average cell population density (ρ_{av}) was computed at indicated sections from three randomly selected scaffolds (n = 3) per study group and the top, middle, bottom sections were denoted as $\rho_{av\text{-}top}$, $\rho_{av\text{-}middle}$, $\rho_{av\text{-}bottom}$, $\rho^{Control}_{av\text{-}top}$, $\rho^{14}_{av\text{-}middle}$, $\rho^{60}_{av\text{-}bottom}$ represent the average cell population densities in the selected sections from control or US-stimulated (14 and 60 kPa) study groups, respectively. $\rho_{av} \times 100 \pm$ SD (n = 3) was plotted for respective sections.

2.5.3. Cell proliferation

Randomly selected scaffolds (n = 3) per study group were incubated with papain digestion buffer (5 mM L-cysteine, 100 mM Na_2HPO_4, 5 mM EDTA, 125 μg ml^{-1} papain, pH 7.5) for 16–18 h at 70 °C [35]. Quant-iT PicoGreen dsDNA assay kit was used to estimate cell proliferation with respect to US application and culture duration. The supernatant was collected and total DNA was measured according to the manufacturer's instructions. The data were presented as average ± SD (n = 3).

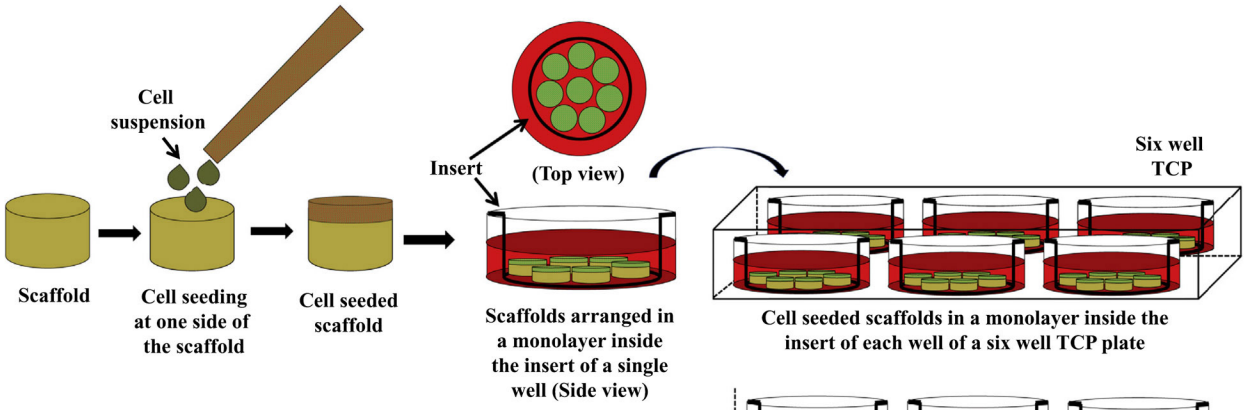

Table 1. Experimental parameters used for culturing construct in US bioreactor for 21 days.

Scaffolds	US regimes	Applications /day	Duration of each application (mins)
CS/ CSB/BM	No US Control	6	5
	2.5 VPP/5 MHz (14 kPa)		
	10 VPP/5 MHz (60 kPa)		

Figure 1. Experimental scheme. Pre-wetted scaffolds were seeded with cells; cell-laden scaffolds were arranged in a single layer inside an insert of a 6-well TCP; each TCP plate was placed in a plate holder that was maintained above the transducer array of the US-assisted bioreactor [29].

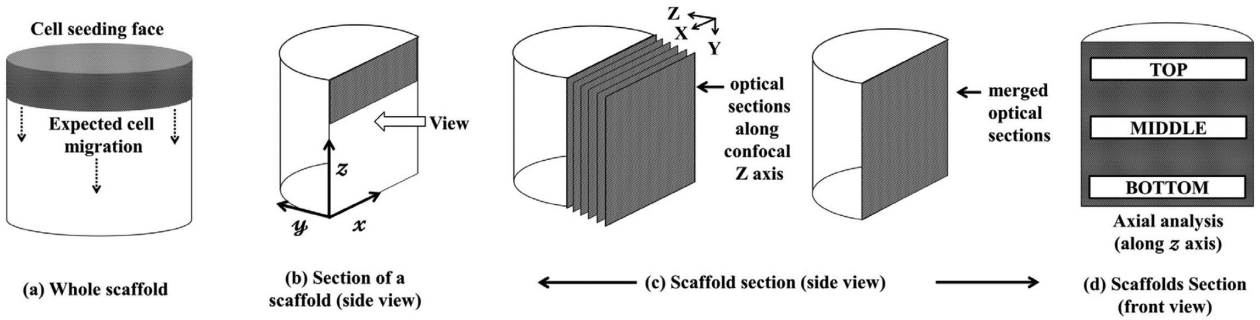

Figure 2. Image analysis scheme. At indicated time points during culture, cell-seeded scaffolds were retrieved, rinsed, fixed and stained with Sytox™. (a) A cylindrically shaped scaffold with cell-seeding face. (b) Scaffolds were cut diametrically in middle (i.e. *x*–*z* plane) and imaged in the indicated direction via confocal microscopy. (c) Optical sections were collected in the confocal Z direction at a step size of 5 μm, merged and imaged at 4× magnification. (d) Merged images were analyzed along the scaffold *x* axis (axial analysis) as depicted. Cell distributions in the selected depth in axial directions were assessed using ImageJ™ 1.46u software and cell numbers per unit area were calculated using the cell counter in the ImageJ™ protocol. Area covered by cells (area covered by cells/total image area) was calculated at three preselected areas along the axial direction and denoted as ρ (cell population at given area).

2.5.4. Cell viability

Pretreatment of scaffolds and live–dead analysis were carried out according to the protocol detailed elsewhere [33]. The cells were visualized by an inverted confocal microscope (Olympus IX81) at the Center of Biotechnology, University of Nebraska–Lincoln. All the images were collected at 20× magnification (z step size = 10 μm).

2.5.5. Cell morphology

The morphology of the chondrocytes in the interior of the scaffolds was observed with VPSEM. Scaffolds were pretreated following the standard procedure [33] and imaged along the *x*–*z* plane (Figure 2b) after cutting the scaffold diametrically in the middle. Areas of interest at different depths in the scaffold interior was designated as R1, R2 or R3, with R1 being close to the seeding face.

2.5.6. RNA extraction and qRT-PCR

At the indicated time point of culture, scaffolds were retrieved, frozen in liquid nitrogen, minced with a tissue grinder, homogenized in Trizol reagent (Invitrogen) and RNA was isolated following standard procedure detailed elsewhere [29]. For qRT-PCR analysis, 40–50 ng of total RNA was added per reaction and assays were carried out in triplicate in an Eppendorf mastercycler realplex RT-PCR system (Eppendorf North America). GAPDH was used as an internal control. Relative gene expressions in US-stimulated samples were analyzed using the $2^{-\Delta\Delta C}{}_T$ method with respect to control (non-stimulated) at every time point. The sequences of GAPDH (Bt03210917_g1), COL1A1 (Bt03225332_m1), COL2A1 (Bt03251843_g1), Aggrecan (Bt03212186_m1), COL10A1 (Bt03215581_m1) TGFβ1 (Bt04259485_m1) and TGFβ3 (Bt03272218_m1) are proprietary to Applied Biosystems Inc. and are not disclosed. Custom-designed primers and probe for Sox-9 have the following sequence: forward primer (GAGACTGCTGAACGAGAG), reverse primer (CGGCTGGTACTTGTAGTC) and Taqman probe (TGGTCCTTCTTGTGCTGCACGC).

2.5.7. Protein isolation and Western blotting analysis

At the end of 21 days of culture, scaffolds were retrieved, frozen in liquid nitrogen, and minced with tissue grinder. Pierce IP lysis buffer supplemented with 1× Halt protease and phosphatase inhibitor cocktail (Thermo Scientific, Rockford, IL) was used to extract protein from the ground scaffolds. A volume equivalent to a total protein of 20 μg of all samples were subjected to SDS–PAGE analysis on a 4–12% NuPAGE Bis-Tris gel (Invitrogen) under denaturing and non-reducing conditions followed by Western blotting to PVDF membrane using the NuPAGE system according to a standard protocol. The membranes were probed with COL1A1 (Santa Cruz Biotechnology; 80565), COL2A1 (ABCAM; ab34712), SOX9 (ABCAM; ab71762), Aggrecan (ABCAM; ab3778) and COL10A1 (ABCAM; ab58632). β-Actin was used as the respective loading control. After washing the membranes with 1× TBST and incubating with respective horseradish peroxidase (HRP)-linked secondary antibodies incubation procedures, protein bands were visualized using an Immun-star HRP substrate kit (Bio-Rad Laboratories, Hercules, CA, USA) and captured with GE Healthcare Amersham Hyperfilm ECL (GE Healthcare, Piscataway, NJ, USA). Each blot was further corrected to minimize blot background with GIMP 2.8.10 software and analyzed with ImageJ™ to compute protein expression. Relative protein expression was computed by normalizing summation of all the bands from each protein expression with respective β-actin expression, and the average expression with standard deviation (n = 3) were presented.

2.5.8. Immunohistochemistry

Cell-seeded constructs were fixed in 4% formalin for 24 h and embedded in paraffin. Sections 15 μm thick were processed using standard histological procedures at the Tissue Science Facility, University of Nebraska Medical Center (Omaha, NE). The primary antibody used for immunofluorescence was rabbit polyclonal collagen II (1:200 dilution; ab34712, Abcam, MA) and the secondary antibody was HRP-conjugated goat anti-rabbit polyclonal antibody (DAKO, K4003).

2.5.9. Statistical analysis

All results were expressed as a mean with standard deviations (SD) for n = 3. One-way analysis of variance (ANOVA) with replication was used to compare all study groups/scaffold type. A pairwise Student's t-test with unequal variance was used to observe significant changes among both the stimulated (14 and 60 kPa) samples with respect to the non-stimulated one at each sampling day and the difference was considered significant when $P < 0.05$, denoted with *.

3. Results

We have identified the primary resonance frequency of chondrocytes to be 5.2 ± 0.8 MHz and at the primary resonance frequency, cells undergo mostly dilatational deformation [35], and this frequency was thus chosen in this study. In order to investigate the effect of different acoustic pressures on cellular response, experiments were carried out at 14 kPa (2.5 Vpp, 5 MHz) and 60 kPa (10.0 Vpp, 5 MHz).

3.1. Scaffold characterization: SEM and MIP

Scaffold morphologies were observed via SEM (Supplementary Figure 1A–C) and the features are summarized in Table 2. CS and CSB scaffolds showed circular to longitudinal macropores with pore diameters ranging from 50 to 300 μm. Circular micropores ranging from 10 to 50 μm were observed on the pore walls of CSB scaffolds, rendering the surface rough. We note that BM scaffolds have circular, open, regular and repetitive macropores ranging from 100 to 500 μm. Percent porosity and pore size distributions (PSDs) ascertained by MIP are also shown in Table 2 and Supplementary Figure 1D–F. The PSDs were observed to be unimodal with mean pore size values of ~44.1 ± 7.4 and ~148.6 ± 6.6 μm for CS and BM, respectively, whereas CSB exhibited a bimodal distribution with major pore size values in the range of 39.0 ± 4.9 μm. Micropores ranging from 5 to 15 μm were only noted in CSB scaffolds. We note that CSB scaffolds have comparatively higher per cent total porosity (82.2 ± 2.2) compared to CS scaffolds (75.2 ± 1.2), with BM scaffolds (93.0 ± 0.1) being the most porous. Similar tortuosity (τ) values were noted for both CS and CSB scaffolds. Among the three scaffolds, BM possessed the lowest tortuosity, 2.9 ± 0.9, which indicated a relatively simpler, interconnected structure.

3.2. Estimation of cell population density and distribution at varying depths in a scaffold

To obtain a baseline for estimations, the initial distribution of cells in the scaffolds tested was evaluated after completion of the cell-seeding step, and prior to commencement of the US exposure (shown in Supplementary Figure 2). In CS scaffolds, cells were restricted to the seeding face. In the case of CSB scaffolds, cells were mostly restricted to the seeding face, with a few cells scattered throughout the scaffold depth. In contrast to CS and CSB scaffolds, BM scaffolds had a rather well-distributed cell population to start with, perhaps owing to their high porosity and low tortuosity.

Cell distribution at the scaffold interior was observed in all the study groups and representative images at the end of days 7 and 21 in culture are shown in Figure 3. Cell population density (ρ_{av}) was computed according to the scheme shown in Figure 2 and presented in Figure 4A. The length of the bar (Figure 4A) serves as an indirect estimation of total number of cells present per unit area (ρ_{av}) at the selected section. The ratio of the lengths of the hatched, clear or solid bars indicative of the top ($\rho_{av\text{-}top}$), middle ($\rho_{av\text{-}middle}$) and bottom $\rho_{av\text{-}bottom}$) cell population density is a measure of the uniformity of cell distribution along the length of the scaffold.

Distinctly different cellular distribution profiles were observed in the three scaffolds evaluated. Cells were mostly localized at the periphery of the CS scaffolds as visualized from the images (Figure 3) and their respective image analysis (Figure 4A). At day 21, both control and US-treated cell-seeded CS scaffolds had similar ρ_{av}($P > 0.1$) at the top, middle and bottom sections of the images, with top sections being predominantly populated ($\rho^{control}_{av\text{-}top}$: $\rho^{14}_{av\text{-}top}$: $\rho^{60}_{av\text{-}top}$ = 1:1:1.5), implying that US stimulation had minimal impact on cell infiltration and distribution on CS scaffolds.

In CSB scaffolds, cells were mostly localized on the periphery at day 1, and with increasing culture duration, cell infiltration into the scaffold depth was observed for both the US regimens evaluated. After 21 days, clusters of cells were observed along the scaffold depth of cell-seeded CSB scaffolds (Figure 3). The ratio of $\rho_{av\text{-}top}$, $\rho_{av\text{-}middle}$, $\rho_{av\text{-}bottom}$ for control and either of the US-stimulated cell-seeded CSB scaffolds were similar (Figure 4A). Notably, ρ_{av} at any given depth was higher for US-treated cell-seeded CSB scaffolds compared to control cell-seeded CSB scaffolds ($P < 0.05$). For example, $\rho_{av\text{-}middle}$ for control, 14 kPa and 60 kPa treated cell-seeded CSB scaffolds were 4.34 ± 0.10, 7.23 ± 0.69, 14.16 ± 5.48, respectively, implying that the US stimulation yielded higher cellular proliferation along the scaffold depth.

US stimulation positively enhanced cellular proliferation and cell population density at all depths evaluated in BM scaffolds when compared to control. At day 21, both control and US-treated BM scaffolds had similar ratios of $\rho_{av\text{-}top}$, $\rho_{av\text{-}middle}$, $\rho_{av\text{-}bottom}$, indicating a uniform depth-independent cellular distribution (Figs. 3 and 4A). The ρ_{av} at any given section was significantly higher ($P < 0.05$) in US-treated BM scaffolds compared to control. Image analysis was also carried out in the radial direction of the scaffold, and similarly US was noted to yield higher cell population density at any given radial depth when compared to controls (data not included). Collectively, the results suggest that US stimulation positively impacted depth-independent cell population density throughout the scaffold volume for both CSB and BM scaffolds, with 60 kPa treatment resulting in higher cell proliferation over 14 kPa.

3.3. Cell proliferation

Cell proliferation was assessed over the culture duration and is shown in Figure 4B. Cell-seeded BM scaffolds have the highest cell proliferation when compared to both cell-seeded CS and CSB at every time point evaluated. Distinctly higher proliferation was noted on both the US (14 or 60 kPa) treated cell-seeded BM scaffold compared to non-stimulated control cell-seeded scaffolds ($P < 0.05$) at the end of days 1, 7, 14 and 21.

Additionally, live–dead staining was used to ascertain cellular viabilities (Supplementary Figure 3). At the end of day 21, US-treated cell-seeded CSB and BM constructs had higher cellular viability compared to their respective controls and both the US-stimulated and control CS scaffolds.

3.4. SEM analysis

Cellular morphology along the scaffold depth (i.e. axial direction) was visualized by SEM in order to gauge the depth-dependent cellular morphological changes between control and US-stimulated study groups. Figure 5 shows the SEM images obtained along the scaffold *z* axis on day 21. In both control and

Table 2. Scaffold characterization with SEM and MIP.

Scaffold type	Dimension diameter × height (mm)	SEM			MIP		
		Macropores (diameter, μm)	Micropores (diameter, μm)	Features	Median pore diameter (μm)	% Porosity	Tortuosity
CS	5 × 2.5	Circular (~60) to longitudinal (~200)	–	Smooth surface; irregularly distributed pores	44.1 ± 7.4	75.2 ± 1.2	4.6 ± 0.6
CSB	5 × 2.5	Circular (~50) to longitudinal (100–300)	Circular (10–50)	Rough surface; irregularly distributed pores	39.0 ± 4.9	82.2 ± 2.2	6.4 ± 3.2
BM	5 × 2.5	Circular (100–500)	–	Smooth surface; regularly distributed pores	148.6 ± 6.6	93.0 ± 0.1	2.9 ± 0.9

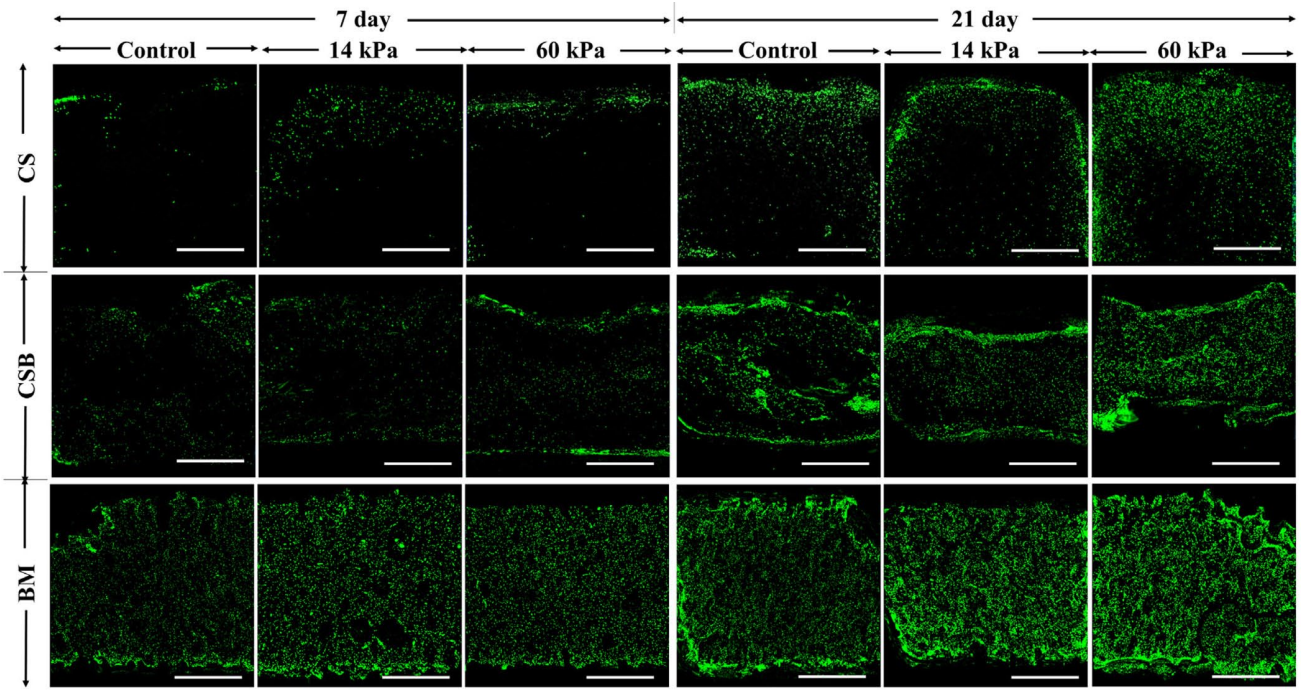

Figure 3. Cellular distribution via confocal imaging. Upon completion of the fixation step and staining with nucleic acid stain Sytox, images were collected at the midsection of the scaffold (Figure 2b) at 4 x magnification (scale bar: 1 mm). Representative images of scaffold interior from days 7 and 21 from all study groups were presented here.

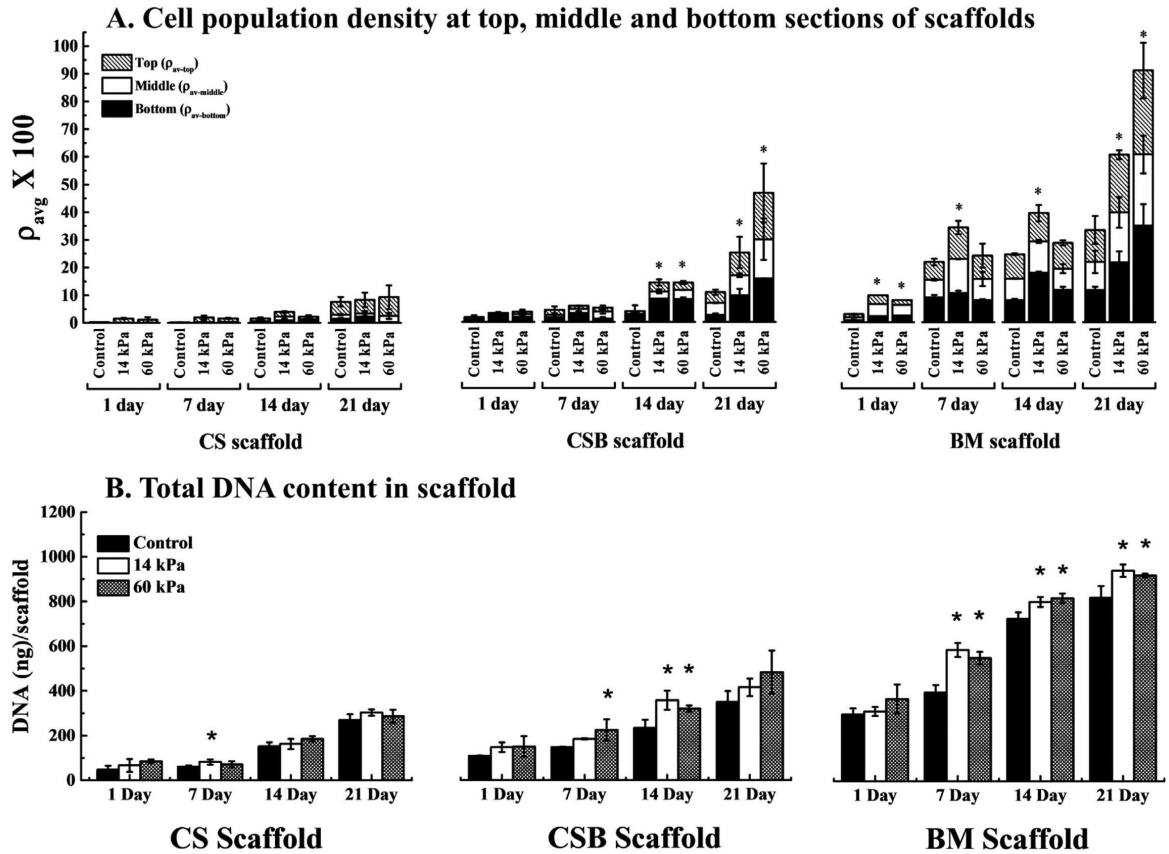

Figure 4. (A) Estimate of cell population density (spatial average cell density, ρ_{av}). Spatial distribution of cells within a construct in the selected sections (Figure 2d) were computed and an average cell population density (ρ_{av}) at respective top, middle and bottom sections (ρ_{av} × 100) ± SD (n = 3) was plotted as a function of day in culture. (B) Cell proliferation measured with standard Quant-iT™ PicoGreen® assay. Total DNA contents were measured on the scaffolds of each study groups and average values ± SD (n = 3) were plotted as a function of time. At each time point, cell proliferation data obtained under US was compared with respective control and, statistically significant data (P < 0.05) are indicated with *. Statistically significant different data between two US conditions are shown in brackets.

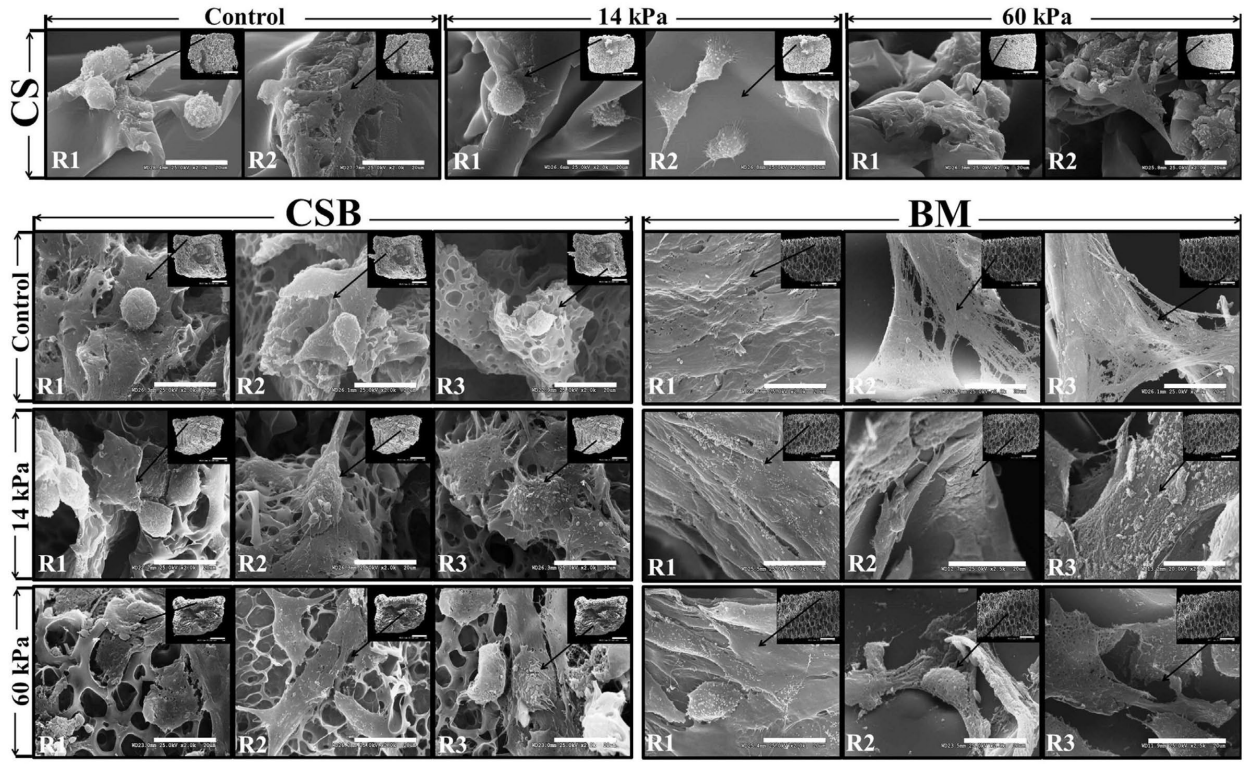

Figure 5. Cellular morphology in the axial direction. Cell morphology at various depths of the scaffold interior was imaged with VPSEM at 2000 x magnification (scale bar: 20 μm) and images from day 21 scaffolds are shown. Inset image depicts an area of interest along the axial direction of the scaffold interior (35–50 x magnification; scale bar: 1 mm) and designated as R1 (top), R2 (middle) and R3 (bottom), where R1 is located close to the cell seeding surface.

US-stimulated cell-seeded CS scaffolds, cell populations were mostly located close to the seeding surface (R1 and R2) and appeared spherical, oval or flat shaped, with few microvilli. Cell projections were observed in US-stimulated cell-seeded CS scaffolds. Cell surfaces on control, non-stimulated CSB scaffold were visibly smooth. In US-treated CSB scaffold, the cellular morphology was observed to be fusiform, with multiple cellular projections in regions R1, R2 and R3.

In both control and US-treated cell-seeded BM scaffolds a subconfluent layer of cells stretching along the pore walls was observed. The cell surfaces on control BM scaffolds were visibly smooth, with a noticeable appearance of elongated, fibrous cell structure in the scaffold interior (R2, R3), possibly corresponding to a dedifferentiated chondrocyte phenotype. In contrast, polygonal, fusiform cell structures embedded in dense matrix were observed in regions R1, R2 and R3 of both 14 and 60 kPa US-treated cell-seeded BM scaffolds. We note that a deviation from a spherical to a fusiform structure is related to the strong adhesive mechanism of cells to the scaffold structure perhaps modulated by US stimulation and associated matrix secretion. We also note that similar chondrocyte structures were observed elsewhere on collagen sponge [36] and do not necessarily imply dedifferentiation.

3.5. Gene expression of cartilage-specific markers

The impact of US stimulation on mRNA expression of chondrocytic markers (COL1A1, COL2A1, ACAN) as a function of culture duration was examined by qRT-PCR. The changes in the relative gene expression of COL2A1 to COL1A1 and aggrecan expression levels as a function of US stimulation and time of culture are shown in Figure 6. In the absence of US, similar relative gene expression of COL1A1, COL2A1, ACAN was observed on all scaffolds tested as a function of culture period. However, compared to control, higher levels of COL2A1/COL1A1 and ACAN expression were observed on US-treated cell-seeded constructs. The gene expression of Sox-9, TGFβ1, TGFβ3 and hypertrophic marker, COL10A1, evaluated on day 21 is shown in Figure 6. Cells stimulated with US had higher mRNA levels of Sox-9 compared to control in all three scaffolds and paralleled COL2A1 expression. We note that both the data in this paper and that reported elsewhere [27] suggest that US stimulation induces the expression of Sox-9 in the absence of exogenously added TGFβ.

3.6. Protein expression analysis by Western blotting

The expression of chondrocytic proteins (COL1A1, COL2A1, ACAN) and transcription factor Sox-9 were assayed by Western blotting (Figure 7A), analyzed with ImageJ™ and the relative expression was computed. Protein expression of COL1A1 was noted to be similar in all groups studied. Higher levels (1.5- to 1.8-fold) of COL2A1 protein expression on US stimulated scaffolds were noted with respect to their control. Notably high Sox-9 and ACAN expression were observed in BM scaffolds under US stimulation compared to its control and either of CS and CSB scaffolds. No COL10A1 expression was noticed on any scaffold.

3.7. IHC analysis for COL2A1 distribution

The distribution of COL2A1 on day 21 was examined by IHC and is shown in Figure 7B. COL2A1 was observed throughout the cross-section in both control and US-treated cell-seeded BM scaffolds. The intensity of COL2A1 stain was visibly higher on BM scaffolds treated with US at 60 kPA when compared to either controls or 14 kPa treatment. In cell-seeded CS and CSB scaffolds, collagen II was mostly restricted to the seeding face and the peripheral region of the constructs.

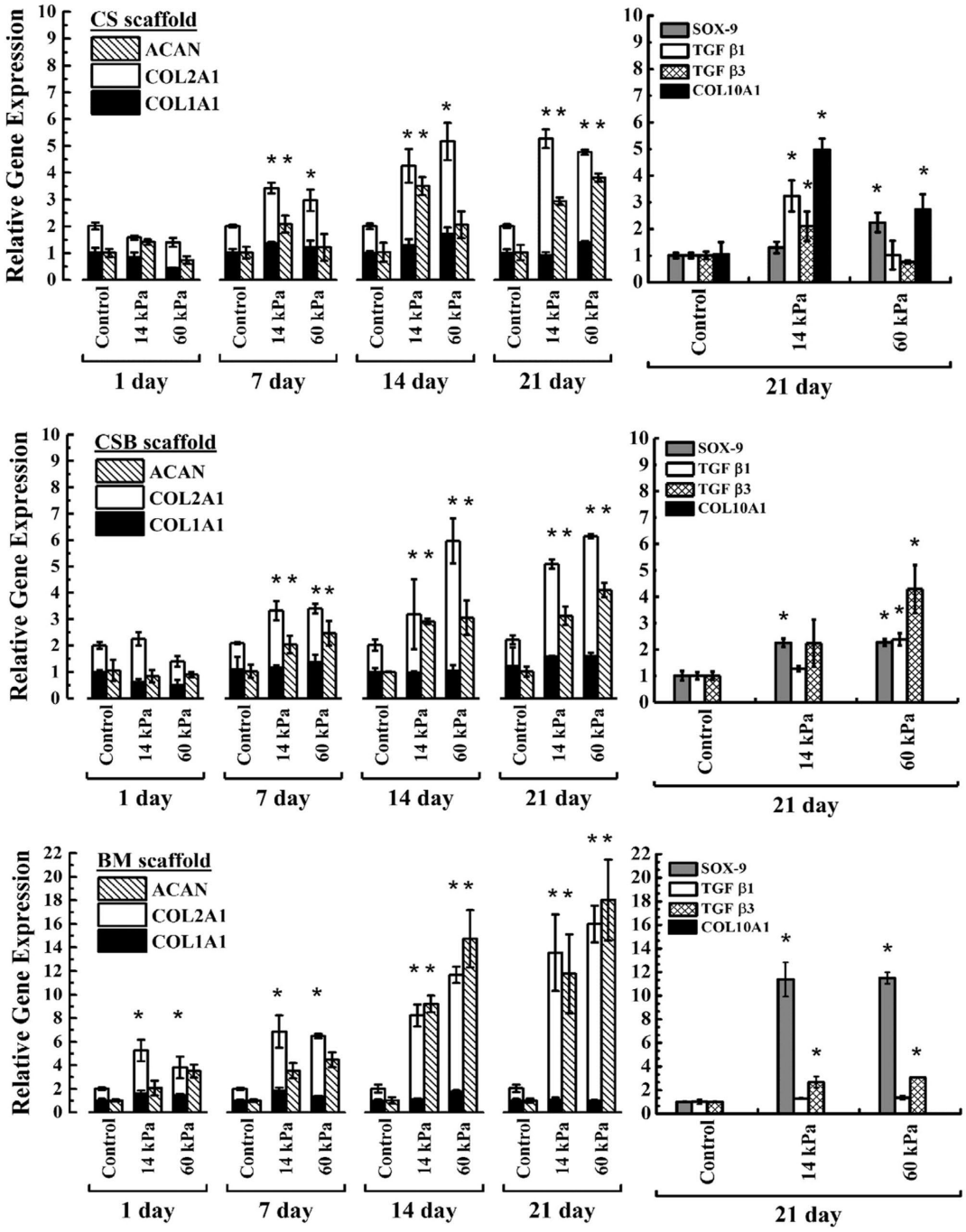

Figure 6. Relative gene expression. Relative gene expression analysis was performed using the $2^{-\Delta\Delta C}{}_T$ method on RNA isolated from cell-seeded constructs at the end of 1, 7, 14 and 21 days of culture. The average values ± SD (n = 3) were reported. Changes in the relative expression of COL2A1 to COL1A1 and Aggrecan as function of culture duration are shown in the left column. Right column depicts mRNA expression for Sox-9, TGFβ1, TGFβ3 and COL10A1 only after 21 days of culture. Top, middle and bottom panels show gene expressions on CS, CSB and BM scaffolds, respectively. At each time point, gene expression data obtained under US was compared with respective controls and, statistically significant data ($P < 0.05$) are indicated with *. Statistically significant different data between two US conditions are shown in brackets.

3.8. Analysis of US field in scaffolds

Our experimental findings support our premise that US stimulation and scaffold architecture impacts depth-dependent cell population density. To better understand the observed results this section presents a brief analysis of the distribution of the US field in the different scaffold types. The air interface above the samples acts as an acoustic reflector and results in the production of an ultrasound standing wave field throughout the sample volume [37]. Recalling that the primary role of US is to impart mechanical stimulation to cells, we recognize two types of mechanical stimulation: (i) shear deformation of cells when velocity gradients are present (and shear wave transference of energy when cells are attached to a solid surface); (ii) mechanical dilatation when a cell located at/near a pressure antinode experiences radial strain.

Scaffolds have porosities in the range of 74–93% comprising either continuous or interrupted pores with thin-walled boundaries (Table 2). Modeling of US propagation or distribution in a scaffold is a highly complex problem mainly due to

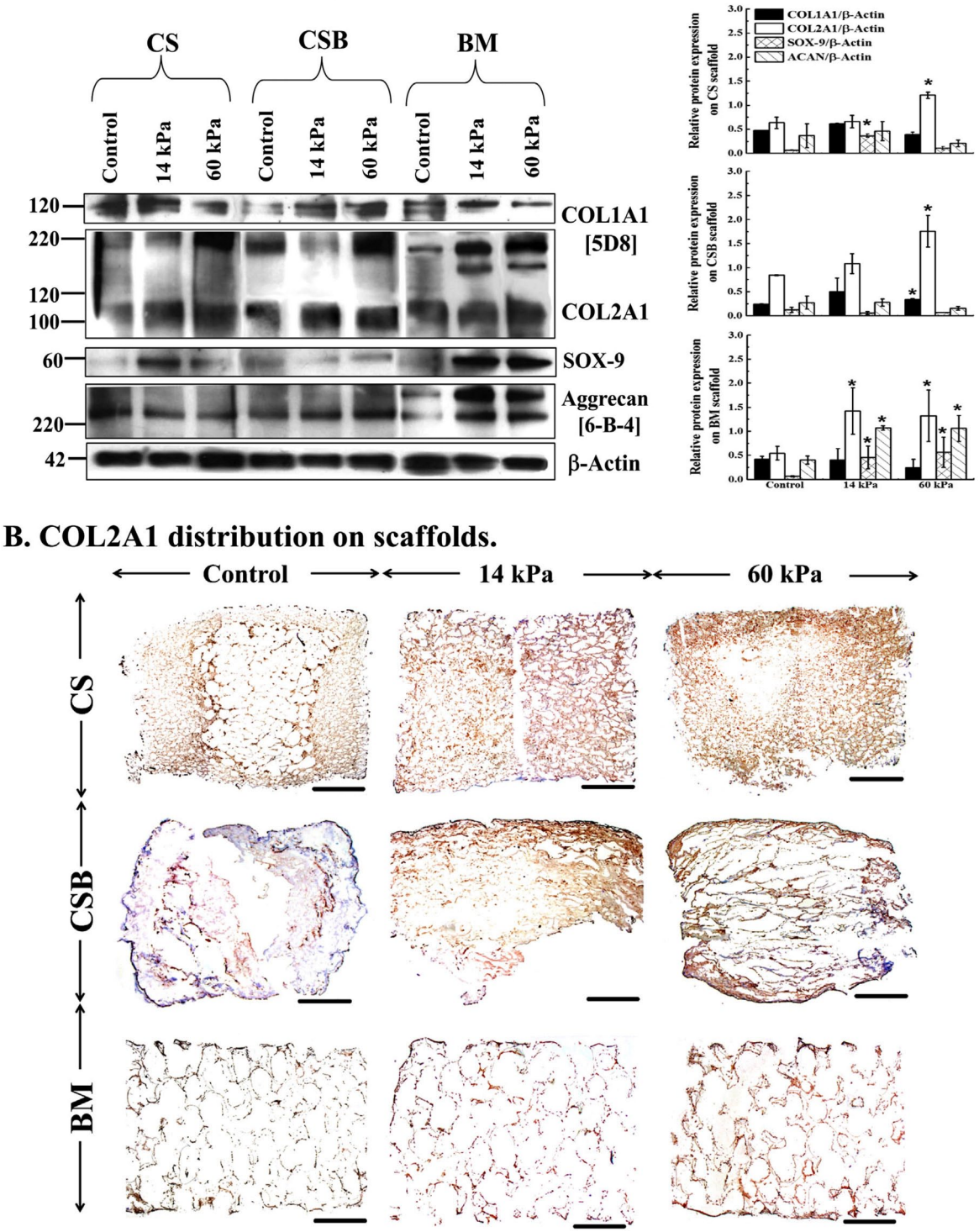

Figure 7. (A) Analysis of protein expression. Protein isolated from cell-seeded CS, CSB and BM scaffolds at the end of 21 days of culture with or without US was subjected to Western blot analysis according to the procedure described, and the bands respective to COL1A1, COL2A1, Sox-9, Aggrecan are shown. β-Actin was used as the loading control. The sum of the bands observed with respect to each protein were further quantified with ImageJ software, normalized with respective β-actin and relative expression was presented ($^*P < 0.05$). (B) COL2A1 distribution on scaffolds at day 21 by IHC. Scaffold sections 15 μm thick, collected from the x–z plane (Figure 2b) of control and US-stimulated groups from day 21, stained with rabbit polyclonal antibody against collagen type II and imaged with a Zeiss AX10 at 2.5× magnification (scale bar: 1 mm).

the heterogeneity of the scaffold architecture and multiphasic nature of the domain. Thus as a first approximation, we incorporate the following assumptions into our modeling effort. Assuming that the solid phase is isotropic, it can support both longitudinal and shear waves. Only longitudinal waves are present in the liquid phase. The US field that is incident on the scaffold only has a velocity component, u_1, parallel to the scaffold axis (i.e. z axis) as shown in Figure 2.

The linear wave equation with viscous effects characterized by the kinematic viscosity v is:

$$\frac{\partial^2 u_1}{\partial t^2} = c_0^2 \frac{\partial^2 u_1}{\partial z^2} + \upsilon \frac{\partial}{\partial t}\left[(1+\eta)\frac{\partial^2 u_1}{\partial z^2} + \frac{\partial^2 u_1}{\partial r^2} + \frac{1}{r}\frac{\partial u_1}{\partial r}\right] \quad (1)$$

where c_0 is the sound velocity and η is the dimensionless bulk modulus. Equation (1) is applicable to fluid and solid media, provided the appropriate material properties are used. Viscosity effects are neglected for the incident field, hence the solution to the reduced Equation (1) (for $\upsilon = 0$) is:

$$u^{inc} = u_0 e^{i\omega t - ikz}$$

where the frequency ω and wavenumber k are related to the sound velocity in the fluid phase as $\omega/k = c_0$ and u_0 is a reference velocity. Transmission, reflection and absorption of acoustic waves in the scaffolds leads to a complex problem that ideally must be solved by finite-element methods, considering the geometry of the solid and fluid phases. In lieu of such a comprehensive analysis, Biot theory is a good compromise [38], because it provides a good description of the macroscopic behavior in the porous medium. However, to obtain insight into the effect of the acoustic field on cells, albeit qualitatively, no homogenization of the porous medium can be applied. SEM images of the three scaffold types as shown in Supplementary Figure 1A–C offer some guidance in the construction of models that maintain the heterogeneous character. If the scaffold is approximated by an assembly of pores, then dampening results primarily from the non-slip condition at the wall. We note that acoustic impedance ($Z = \rho \times c_0$, where ρ is density) of the fluid (denoted as f) and solid phases (denoted as s) do not differ much ((Zs/Zf = 1.28)). Thus, both compressional and shear waves will exist in the solid phase, but perhaps the solid phase's most important effect on fluid motion is the attenuation of acoustic waves due to non-slip conditions at interfaces. We estimate representative pore diameters of the different scaffolds using porosity data, a measure of solid to fluid volumes. It is important to note that the pore diameter range overlaps with the wavelengths of US in water—US transmission is drastically affected if wavelengths are shorter than the pore diameters [39]. Defining the pore radius as Φ, porosity as ϵ_p and the average thickness of solid structures as Δt, we relate Φ to ϵ_p as $\Phi = (2\Delta t\varepsilon_p) \div (1\text{-}\varepsilon_p)$. We use the same thickness for all scaffolds, and estimate it from setting the median pore radius for the most porous scaffold equal to Φ. Using the value of Φ = 75 μm for the BM scaffold, we estimate the average thickness as 2.8 μm Thus, the pore radii for CSB and CS scaffolds are Φ_{CS} = 16.8 μm and Φ_{CSB} = 25.5 μm and these values were used in subsequent analysis. Two points are noteworthy: (i) all three estimates of pore diameters are smaller than the US wavelength of ~300 μm and (ii) this analysis differs from the classical Kirchoff problem (sound propagation in a perfectly stationary circular tube),

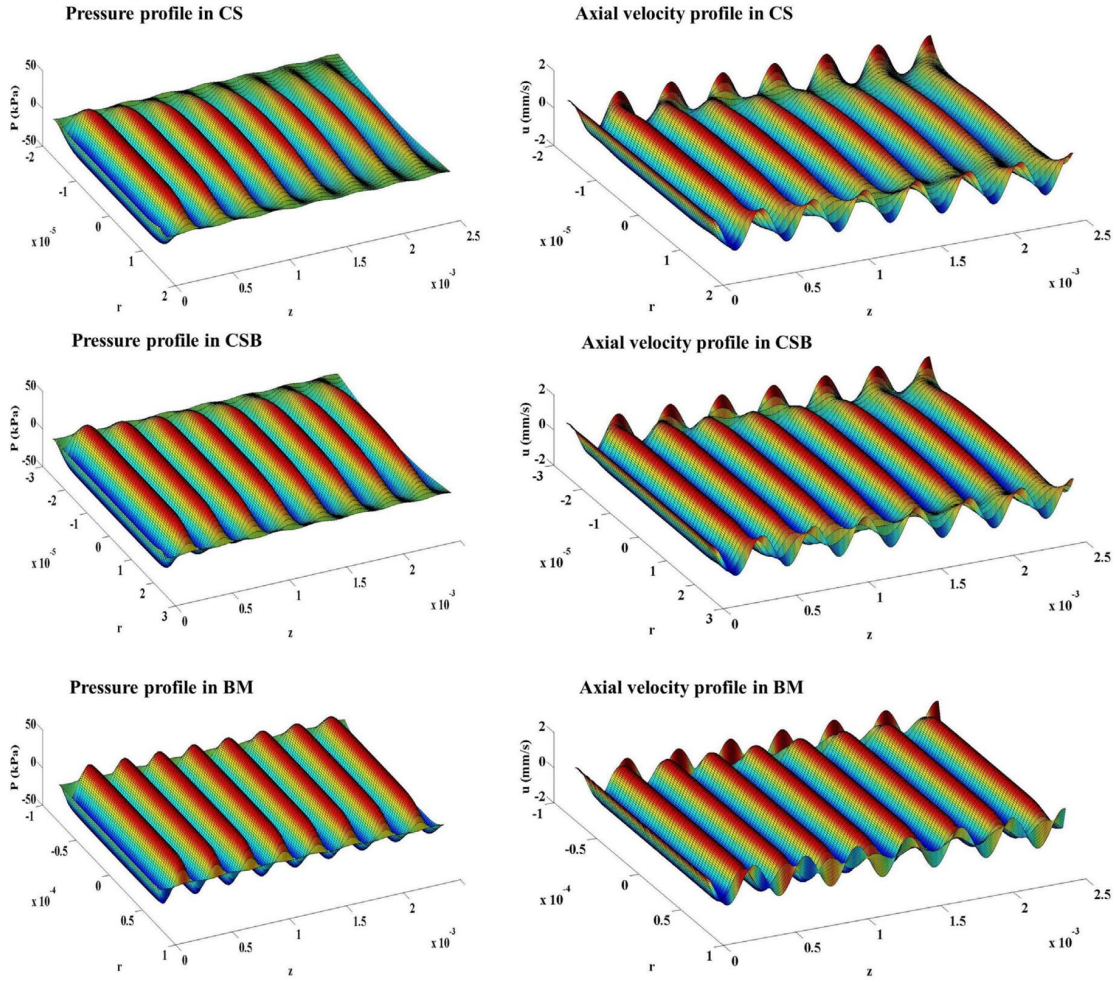

Figure 8. Mathematical model results showing pressure and axial velocity profiles in the scaffolds. The left and right panels show the pressure and the axial velocity, respectively, in a typical pore of the CS, CSB and BM scaffolds. The plots are presented in perspective and the transducer is positioned to the left ($z < 0$; therefore, the incident field approaches from the left, and increased attenuation is observed as z increases. Note the velocity at the lateral wall due to motion of the solid phase. The differences in propagation properties place these waves out-of-phase with the fluid phase (shown in all three figures in the second column).

because we include wave propagation in the solid phase and the coupling of acoustic motion in the solid phase with the fluid phase. The solution to Eq. (1) for acoustic motion in a single pore consists of two parts. The first part of the solution

$$u_{11} = e^{i\omega t}\sum A_n J_0(\lambda_n r)e^{-ik_n z} \quad (2)$$

solves the problem as if the walls (solid phase) are completely stationary; thus, the values λ_n are the roots of the zero-order Bessel function of the first kind, $J_0(\lambda_n\Phi)=0$. Wavenumbers k_n are determined by the dispersion relation:

$$\omega^2 = c_0^2 k_n^2 + i\omega\nu[(1+\eta)k_n^2 + \lambda_n^2].$$

The second part of the solution is a result of the incident acoustic waves that create an US field in the solid phase such that the compressional waves in this phase have the same frequency as the incident field, but the wavenumber differs:

$$v^{wall} = Be^{i\omega t - ik_s z} - B'e^{i\omega t + ik_s z}$$

($\omega/k_s = c_s$). Both forward and reverse traveling waves are present in the solid phase due to transmission/reflection at $z = 0$, L. Thus, the second part of the solution is an evanescent wave that is driven by the wall motion (I_0 is the modified Bessel function of the first kind of order zero):

$$u_{12} = e^{i\omega t} I_0(\beta r)[Ce^{-ik_s z} - C'e^{ik_s z}]$$

where $\beta^2 = i\omega/\nu + k_2^s(1+\eta)$ and $C = B/I_0(\beta\Phi)$, $C' = B'/I_0(\beta\Phi)$. The inlet condition is:

$$u_{11} + u_{12} = v^{inc}$$

at $z = 0$. The coefficients A_n are determined by projection:

$$A_n = \frac{2\int rJ_0(\lambda_n r)(\varepsilon - (C - C')I_0(\beta r))dr}{(\Phi J_1(\lambda_n\Phi))^2}$$

Our main result is the following explicit expression for density ρ_1 (and pressure P_1):

$$\rho_1 = P_1/c_0^2 = \frac{\rho_0}{\omega}e^{i\omega t}\left[\sum A_n k_n J_0(\lambda_n r)e^{-ik_n z} + I_0(\beta r)k_s(Ce^{-ik_s z} + C'e^{ik_s z})\right]$$

Figure 8 shows the pressure P_1 and axial velocity u_1 for CS, CSB and BM scaffolds, respectively. Dampening was progressively stronger in the CSB and CS scaffolds due to the smaller pore radii. The analysis provides us with a qualitative comparison between the scaffolds. The US field was strongest in the BM scaffold, weaker in the CSB scaffold and weakest in the CS scaffold; based on the pressure fields in Figure 8 we expect better mechanical stimulation in the BM scaffold, less in the CSB and least in the CS scaffold.

4. Discussion

The creation of a homogeneous tissue without aggregation or pockets of necrosis as a result of nutrient depletion is an important objective of a successful engineering strategy. Non-homogeneity can arise from: (i) non-uniform distribution of cells in the hydrogel or scaffold, and (ii) diffusional limitations of nutrients/factors. While the ultimate goal is to generate tissue-engineered cartilage in these bioreactors, this paper focused on ascertaining the ability of the US-assisted bioreactors both to afford and support a uniform cell distribution and to maintain chondrogenic differentiation.

Low-intensity pulsed US (1.5 MHz, 1.0 kHz repeat, 6–40 min) has been previously employed to stimulate in vitro chondrocyte cultures [40–42]. As a significant departure from such strategies, we have employed low-intensity continuous US to stimulate chondrocytes seeded in 3-D matrices at 5.0 MHz, the primary resonant frequency [37, 43]. At the primary resonance frequency, cells undergo mostly dilatational deformation, and stress gradients are greatest around the nuclear envelope, facilitating mechanotransduction [43].

4.1. Impact of US on proliferation and cell population density (ρ_{av})

To demonstrate the broad applicability of the US-assisted bioreactor that we have developed, we included scaffolds of differing porosities, pore sizes and pore architectures (Table 2, Supplementary Figure 1). The total DNA content was relatively higher in US-stimulated CSB and BM scaffolds compared to non-stimulated controls. For CSB and BM scaffolds, culturing in the US-assisted bioreactor resulted in notable improvements in cell population densities over non-stimulated controls at any given depth along the scaffold z direction (Figure 2). Given the open pore structure of the BM scaffold, cell uniformity was significantly higher in BM compared to CSB and CS (BM ≫ CSB > CS), even in static controls. Even though the ratio of ρ_{av} at selected top, middle and bottom sections was similar in control and US-stimulated BM scaffolds, at any given depth US-treated scaffolds had significantly higher ρ_{av} compared to non-stimulated control. Our collective findings indicate that the increase in cell proliferation is US specific and related to the spatial architecture of scaffold.

Our observations were based on the persistence of the acoustic field over most of the radial surface, even along the length of the scaffold and dependence of the attenuation of US stimulation in the scaffold on porosities, pore sizes and pore architectures. To better explain and understand the distribution of the US field in the scaffolds, an acoustic model was developed in which the propagation of the US field was assumed to be one-dimensional, parallel to the scaffold-axis, and the scaffold parameters such as porosity and tortuosity were accounted for. The model analysis provides a degree of comparison, albeit qualitative, between the scaffolds. Nonetheless, we were able to undertake a qualitative comparison between scaffolds at the opposite side to the incident field for consistency with the experimental setup. Our acoustic model predicted that in a macroporous matrix such as Biomerix™ (pore size ~140 μm, Table 2), the attenuation of the US signal was less and the acoustic field persisted over most of the radial surface even near the outlet. Thus, cells on BM scaffold were able to respond to a uniform US field compared to both CS and CSB scaffolds where US signal was attenuated.

The absence of cell bands in the scaffold does not imply the absence of a standing wave field. Firstly, the seeded cells are anchored and therefore not subject to movement under acoustic radiation, and secondly, the standing wave field depends (very sensitively) on the height of the water column above the scaffold, hence minute variations in the height (e.g. evaporation) lead to changes in the positions of nodes and anti-nodes [37, 44]. Consequently, on the time scale of cell mitosis, the acoustic field has varied between pressure node and anti-nodes at any specific scaffold position.

Even though our paper evaluated the efficacy of a US-assisted bioreactor to sustain cellularity and cellular activity in cylindrical scaffolds with an effective diameter of 22 mm and thickness of 2.5 mm that were statically seeded on the top face by design (Figure 1), in the absence of an effective scaffold structure that promotes cell access and cell stimulation through the scaffold cross-section, we anticipate peripheral colonization along with a sparsely populated scaffold midsection with varying cellular morphology along the scaffold axis coupled with a low level of chondrocytic markers. While the use of BM, a macroporous scaffold with low tortuosity and interconnected pore

architecture enabled a uniform cell distribution to begin with, the greater overall proliferation with higher depth-independent cell densities and cellular activity noted under US stimulation was perhaps due to the inherent ability of the scaffolds to better modulate the US field within the scaffold and offer uniform stimulation through the scaffold volume. As a thicker scaffold is not expected to attenuate the US field [37], we suggest that future research should focus on the ability to generate larger constructs (e.g. 10 mm × 40 mm).

4.2. Biosynthetic response to US

Chondrocytes when expanded in monolayer cultures experience a rapid decrease in COL2A1/COL1A1 ratio and typically at a late passage in 2-D culture (>passage 10) a COL2A1/COL1A1 ratio of 0.5 was noted [45]. We have used COL2A1/COL1A1 ratio as a metric to improve our understanding of the process of chondrocyte differentiation under US (Figure 6). In this paper, the transition of articular chondrocytes from the spherical morphology to the flattened morphology was accompanied by changes in the patterns of collagen expression, and was dependent on the type of scaffold employed. In Biomerix™ scaffolds, where the US signal was least attenuated, thereby affording US-assisted cell dilatation, we observed that the COL2A1/COL1A1 ratio increased with days in culture, with a maximum value of 15/1 obtained at day 21. Collectively, protein expression data corroborates the gene expression analysis. In CS and CSB scaffolds, the maximum value of the COL2A1/COL1A1 ratio ~5/1 was obtained at day 21. The starting P3 BAC cells in our experiment had a COL2A1/COL1A1 ratio of 1. Thus US aids in the maintenance of the chondrocyte phenotype over scaffolds for 21 days and promotes the increased expression of chondrocytic markers. Notably, this response to US is dependent on the pore structure of the scaffold and its ability to modulate the US field within the scaffold (Figure 6).

The induction of TGFβ1 mRNA expression by shear fluid flow and in vitro compressive loading has been previously reported [46]. We surmise that TGFβ mRNA was upregulated under the US stimulation regimen employed and was thus assayed at day 21 only. We also observed a 2- to 3-fold higher expression of TGFβ3 mRNA in cells isolated from US-stimulated BM scaffolds compared to non-stimulated controls, and that mRNA expression of TGFβ1was unchanged. As compared to non-stimulated controls, gene expression of Sox-9 mRNA was elevated and paralleled COL2A1 expression. Future studies will test the hypothesis that this combination of regulatory mechanisms, US-sensitive induction of TGFβ3 transcription and post-translational TGFβ3 activation contributes to the specific chondroinduction in cultured chondrocytes under US.

One caveat of this paper is the overall isolation of mRNA performed on pooled cells in culture. Therefore, these results cannot account for individual differences in the rates of dedifferentiation of cells at various depths along scaffold heights. To overcome this limitation, future research will use Col-2a-luciferase reporter gene transformed chondrocytes to investigate the depth-independent differentiation of anchored chondrocytes on scaffolds under US. Future work will also focus on the modeling of obliquely incident waves on scaffolds and to account for the reflection and transmission of US waves in porous scaffolds.

5. Conclusion

This paper has demonstrated that US: (i) enhances the depth-independent cell densities in scaffolds; (ii) stimulates the proliferation of adult chondrocytes; (iii) aids in the maintenance of the chondrocyte phenotype over scaffolds for 21 days and promotes the increased expression of chondrocytic markers; (iv) increases the gene and protein expression of Sox-9 (Collagen-II transcription factor) in the absence of exogenously added growth factors; and (v) selectively enhances the gene expression of TGFβ3 over TGFβ1.

Acknowledgments – This work was supported in part by the American Recovery and Reinvestment Act of 2009 research grant 1R21RR024437-01A1 from the Department of Health and Human Services and Stem Cell-2012-08 from the Nebraska Department of Health and Human Services. We thank Teresa Fangman from the Morrison Microscopy Core Research Facility at the University of Nebraska–Lincoln; Aubre Phillips from the Tissue Science Facility at University of Nebraska Medical Center; and Tuesday Kuykendall from Materials Science & Engineering Lab, University of Washington for technical assistance. We also thank the Nebraska Research Initiative and the UNL Center for Biotechnology for support.

Supplementary Figures 1–3 *follow the* ***References****.*

References

[1] Liu C, Toma IC, Mastrogiacomo M, Krettek C, von Lewinski G, Jagodzinski M. Meniscus reconstruction: today's achievements and premises for the future. Arch Orthop Trauma Surg 2013; 133:95–109.

[2] Mhashilkar AM, Atala A. Advent and maturation of regenerative medicine. Curr Stem Cell Res Ther 2012; 7:430–45.

[3] Boeckel DG, Shinkai RS, Grossi ML, Teixeira ER. Cell culture-based tissue engineering as an alternative to bone grafts in implant dentistry: a literature review. J Oral Implantol 2012; 38(Spec No):538–45.

[4] Huey DJ, Hu JC, Athanasiou KA. Unlike bone, cartilage regeneration remains elusive. Science 2012; 338:917–21.

[5] Paige KT, Vacanti CA. Engineering new tissue: formation of neo-cartilage. Tissue Eng 1995; 1:97–106.

[6] From stem cells to tissue-specific differentiation. Minim Invasive Ther Allied Technol 2002; 11:101–5.

[7] O'Connell GD, Lima EG, Bian L, Chahine NO, Albro MB, Cook JL, et al. Toward engineering a biological joint replacement. J Knee Surg 2012; 25:187–96.

[8] Melero-Martin JM, Dowling MA, Smith M, Al-Rubeai M. Expansion of chondroprogenitor cells on macroporous microcarriers as an alternative to conventional monolayer systems. Biomaterials 2006; 27:2970–9.

[9] Sabatino MA, Santoro R, Gueven S, Jaquiery C, Wendt DJ, Martin I, et al. Cartilage graft engineering by co-culturing primary human articular chondrocytes with human bone marrow stromal cells. J Tissue Eng Regen Med 2012. doi: 10.1002/term.1661.

[10] Filardo G, Kon E, Roffi A, Di Martino A, Marcacci M. Scaffold-based repair for cartilage healing: a systematic review and technical note. Arthroscopy 2013; 29:174–86.

[11] Melchels FP, Tonnarelli B, Olivares AL, Martin I, Lacroix D, Feijen J, et al. The influence of the scaffold design on the distribution of adhering cells after perfusion cell seeding. Biomaterials 2011; 32:2878–84.

[12] Yeatts AB, Choquette DT, Fisher JP. Bioreactors to influence stem cell fate: augmentation of mesenchymal stem cell signaling pathways via dynamic culture systems. Biochim Biophys Acta 2013; 1830:2470–80.

[13] Sun Y, Chen CS, Fu J. Forcing stem cells to behave: a biophysical perspective of the cellular microenvironment. Annu Rev Biophys 2012; 41:519–42.

[14] Santoro R, Olivares AL, Brans G, Wirz D, Longinotti C, Lacroix D, et al. Bioreactor based engineering of large-scale human cartilage grafts for joint resurfacing. Biomaterials 2010; 31:8946–52.

[15] Mabvuure N, Hindocha S, Khan WS. The role of bioreactors in cartilage tissue engineering. Curr Stem Cell Res Ther 2012; 7:287–92.

[16] Vunjak-Novakovic G, Martin I, Obradovic B, Treppo S, Grodzinsky AJ, Langer R, et al. Bioreactor cultivation conditions modulate the composition and mechanical properties of tissue-engineered cartilage. J Orthop Res 1999; 17:130–8. S. Guha Thakurta et al. / Acta Biomaterialia 10 (2014) 4798–4810 4809

[17] Izadifar Z, Chen X, Kulyk W. Strategic design and fabrication of engineered scaffolds for articular cartilage repair. J Funct Biomater 2012; 3:799–838.

[18] Wendt D, Marsano A, Jakob M, Heberer M, Martin I. Oscillating perfusion of cell suspensions through three-dimensional scaffolds enhances cell seeding efficiency and uniformity. Biotechnol Bioeng 2003; 84:205–14.

[19] Wendt D, Stroebel S, Jakob M, John GT, Martin I. Uniform tissues engineered by seeding and culturing cells in 3D scaffolds under perfusion at defined oxygen tensions. Biorheology 2006; 43:481–8.

[20] Freed LE, Hollander AP, Martin I, Barry JR, Langer R, Vunjak-Novakovic G. Chondrogenesis in a cell-polymer-bioreactor system. Exp Cell Res 1998; 240:58–65.

[21] Thevenot P, Nair A, Dey J, Yang J, Tang L. Method to analyze three-dimensional cell distribution and infiltration in degradable scaffolds. Tissue Eng Part C Methods 2008; 14:319–31.

[22] Vunjak-Novakovic G, Obradovic B, Martin I, Bursac PM, Langer R, Freed LE. Dynamic cell seeding of polymer scaffolds for cartilage tissue engineering. Biotechnol Prog 1998; 14:193–202.

[23] Detzel CJ, Van Wie BJ. Use of a centrifugal bioreactor for cartilaginous tissue formation from isolated chondrocytes. Biotechnol Prog 2011; 27:451–9.

[24] Martin I, Obradovic B, Treppo S, Grodzinsky AJ, Langer R, Freed LE, et al. Modulation of the mechanical properties of tissue engineered cartilage. Biorheology 2000; 37:141–7.

[25] Pazzano D, Mercier KA, Moran JM, Fong SS, DiBiasio DD, Rulfs JX, et al. Comparison of chondrogenesis in static and perfused bioreactor culture. Biotechnol Prog 2000; 16:893–6.

[26] Mizuno S, Allemann F, Glowacki J. Effects of medium perfusion on matrix production by bovine chondrocytes in three-dimensional collagen sponges. J Biomed Mater Res 2001; 56:368–75.

[27] Whitney NP, Lamb AC, Louw TM, Subramanian A. Integrin-mediated mechanotransduction pathway of low-intensity continuous ultrasound in human chondrocytes. Ultrasound Med Biol 2012; 38:1734–43.

[28] Hasanova GI, Noriega SE, Mamedov TG, Guha Thakurta S, Turner JA, Subramanian A. The effect of ultrasound stimulation on the gene and protein expression of chondrocytes seeded in chitosan scaffolds. J Tissue Eng Regen Med 2011; 5:815–22.

[29] Subramanian A, Turner JA, Budhiraja G, Guha Thakurta S, Whitney NP, Nudurupati SS. Ultrasonic bioreactor as a platform for studying cellular response. Tissue Eng Part C Methods 2013; 19:244–55.

[30] Madihally SV, Matthew HW. Porous chitosan scaffolds for tissue engineering. Biomaterials 1999; 20:1133–42.

[31] Subramanian A, Lin HY. Crosslinked chitosan: its physical properties and the effects of matrix stiffness on chondrocyte cell morphology and proliferation. J Biomed Mater Res, Part A 2005; 75:742–53.

[32] Chun HJ, Kim GW, Kim CH. Fabrication of porous chitosan scaffold in order to improve biocompatibility. J Phys Chem Solids 2008; 69:1573–6.

[33] Noriega S, Mamedov T, Turner JA, Subramanian A. Intermittent applications of continuous ultrasound on the viability, proliferation, morphology, and matrix production of chondrocytes in 3D matrices. Tissue Eng 2007; 13:611–8.

[34] Reinking L. Examples of image analysis using ImageJ. Bethesda, Maryland, USA: National Institutes of Health; 2007.

[35] Louw T, Whitney S, Subramanian A, Viljoen H. Forced wave motion with internal and boundary damping. J Appl Phys 2012; 111:14702–147028.

[36] Nuernberger S, Cyran N, Albrecht C, Redl H, Vecsei V, Marlovits S. The influence of scaffold architecture on chondrocyte distribution and behavior in matrixassociated chondrocyte transplantation grafts. Biomaterials 2011; 32:1032–40.

[37] Louw TM. Mathematical modeling of ultrasound in tissue engineering: from bioreactors to the cellular scale. Lincoln, NE: University of Nebraska–Lincoln; 2013.

[38] Allard JF, Atalla N. Propagation of sound in porous media: modelling sound absorbing materials. 2nd ed. Hoboken, NJ and Oxford: Wiley-Blackwell; 2009.

[39] Luppe F, Conoir JM, Franklin H. Scattering by a fluid cylinder in a porous medium: application to trabecular bone. J Acoust Soc Am 2002; 111:2573–82.

[40] Parvizi J, Wu CC, Lewallen DG, Greenleaf JF, Bolander ME. Low-intensity ultrasound stimulates proteoglycan synthesis in rat chondrocytes by increasing aggrecan gene expression. J Orthop Res 1999; 17:488–94.

[41] Nishikori T, Ochi M, Uchio Y, Maniwa S, Kataoka H, Kawasaki K, et al. Effects of low-intensity pulsed ultrasound on proliferation and chondroitin sulfate synthesis of cultured chondrocytes embedded in Atelocollagen_ gel. J Biomed Mater Res 2001; 59:201–6.

[42] Zhang Z-J, Huckle J, Francomano CA, Spencer RGS. The effects of pulsed lowintensity ultrasound on chondrocyte viability, proliferation, gene expression and matrix production. Ultrasound Med Biol 2003; 29:1645–51.

[43] Louw TM, Budhiraja G, Viljoen HJ, Subramanian A. Mechanotransduction of ultrasound is frequency dependent below the cavitation threshold. Ultrasound Med Biol 2013; 2013:1303–19.

[44] Leskinen JJ, Hynynen K. Study of factors affecting the magnitude and nature of ultrasound exposure with in vitro set-ups. Ultrasound Med Biol 2012; 38:777–94.

[45] Hamada T, Sakai T, Hiraiwa H, Nakashima M, Ono Y, Mitsuyama H, et al. Surface markers and gene expression to characterize the differentiation of monolayer expanded human articular chondrocytes. Nagoya J Med Sci 2013; 75:101–11.

[46] Streuli CH, Schmidhauser C, Kobrin M, Bissell MJ, Derynck R. Extracellular matrix regulates expression of the TGF-beta 1 gene. J Cell Biol 1993; 120:253–60.

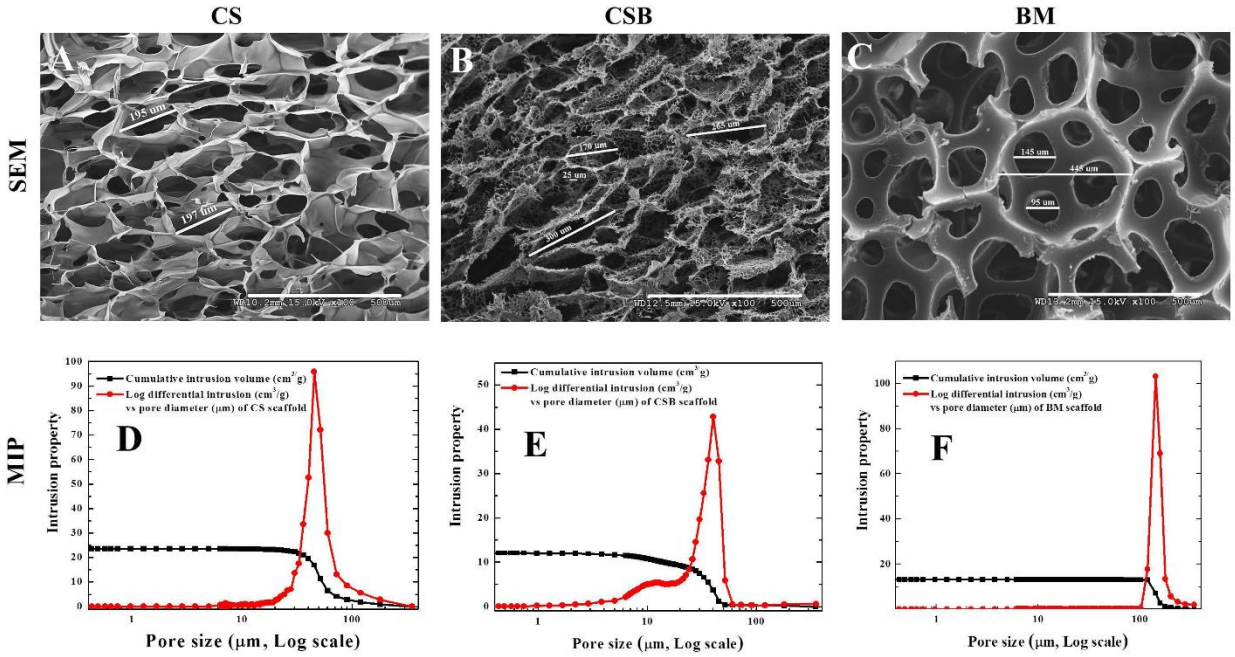

Supplementary figure 1. Scaffold Characterization: Morphology of the scaffold was obtained via VPSEM at 100X magnification (scalebar: 500 μ) and depicted in A-C. Pore size distribution was obtained via mercury intrusion porosimetry and depicted in images D-F. CS: chitosan; CSB: chitosan-10% n-butanol; BM: Biomerix^{TM} scaffolds.

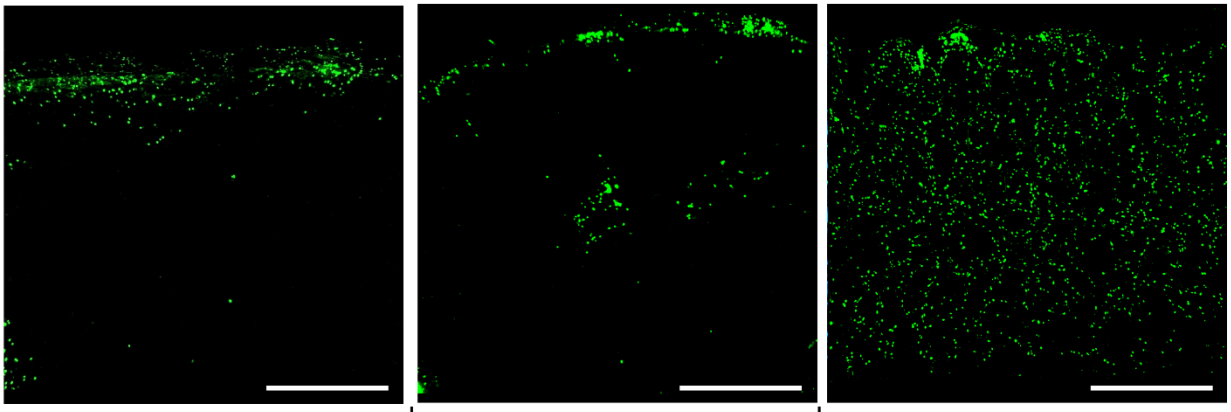

Supplementary Figure 2. Cellular distribution on CS, CSB and BM scaffold via confocal imaging at day 0 before onset of US application.

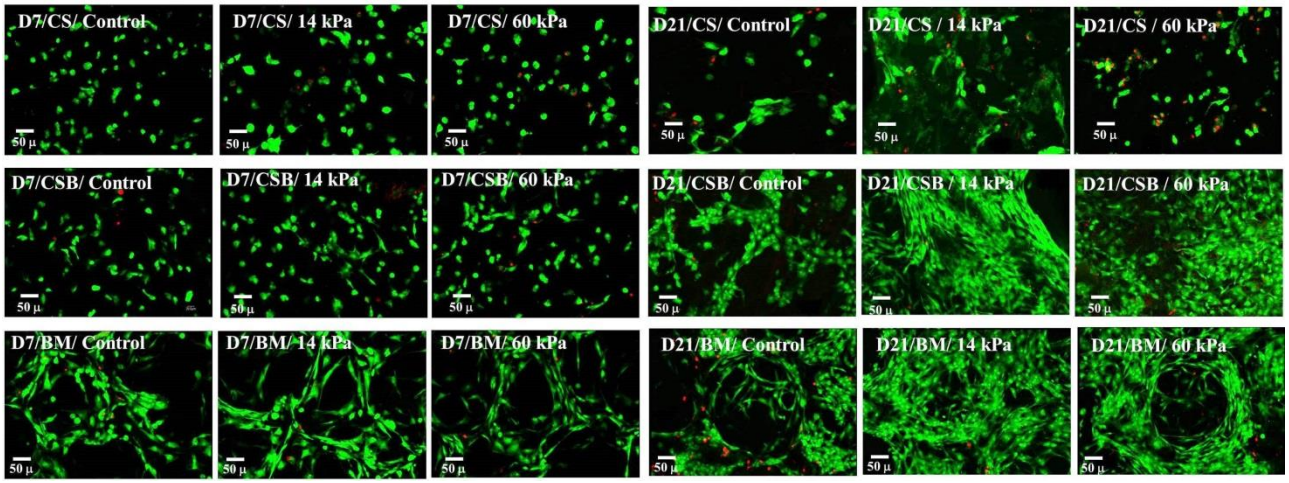

Supplementary Figure 3. Live dead assay of BAC seeded CS, CSB and BM scaffold on 21 days of culture (live cells appearing green and dead cells as read).